JBC RESEARCH ARTICLE

Alpha-hydroxytropolones are noncompetitive inhibitors of human RNase H1 that bind to the active site and modulate substrate binding

Received for publication, December 12, 2021, and in revised form, February 24, 2022 Published, Papers in Press, March 3, 2022,
https://doi.org/10.1016/j.jbc.2022.101790

Nathan L. Ponzar[1,2], **Razia Tajwar**[1,2], **Nicola Pozzi**[2,3], **and John E. Tavis**[1,2,4,*]

From the [1]*Department of Molecular Microbiology and Immunology,* [2]*Institute for Drug and Biotherapeutic Innovation, and* [3]*Department of Biochemistry and Molecular Biology, Saint Louis University, Saint Louis, Missouri USA;* [4]*Liver Center, Saint Louis, Missouri USA*

Edited by Craig Cameron

The ribonucleases H (RNases H) of HIV and hepatitis B virus are type 1 RNases H that are promising drug targets because inhibiting their activity blocks viral replication. Eukaryotic ribonuclease H1 (RNase H1) is an essential protein and a probable off-target enzyme for viral RNase H inhibitors. α-hydroxytropolones (αHTs) are a class of anti-RNase H inhibitors that can inhibit the HIV, hepatitis B virus, and human RNases H1; however, it is unclear how these inhibitors could be developed to distinguish between these enzymes. To accelerate the development of selective RNase H inhibitors, we performed biochemical and kinetic studies on the human enzyme, which was recombinantly expressed in *Escherichia coli*. Size-exclusion chromatography showed that free RNase H1 is monomeric and forms a 2:1 complex with a substrate of 12 bp. FRET heteroduplex cleavage assays were used to test inhibition of RNase H1 in steady-state kinetics by two structurally diverse αHTs, 110 and 404. We determined that turnover rate was reduced, but inhibition was not competitive with substrate, despite inhibitor binding to the active site. Given the compounds' reversible binding to the active site, we concluded that traditional noncompetitive and mixed inhibition mechanisms are unlikely. Instead, we propose a model in which, by binding to the active site, αHTs stabilize an inactive enzyme–substrate–inhibitor complex. This new model clarifies the mechanism of action of αHTs against RNase H1 and will aid the development of RNase H inhibitors selective for the viral enzymes.

Ribonuclease H1 (RNase H1) is a metallonuclease specific for RNA in RNA–DNA hybrids. It plays key roles in nucleic acid metabolism in the nucleus and mitochondria, where it processes R-loops and the RNA primer for mitochondrial replication (1). RNase H1 knockout is embryonically lethal in mice because of failure of the mitochondria to replicate (2).

RNase H1 requires two divalent metal ions, usually Mg^{2+} (Mg_A^{2+} and Mg_B^{2+}) to cleave RNA–DNA hybrids (3, 4). The divalent cations are bound to the enzyme adjacent to one another by the four carboxylate residues comprising the "aspartic acid, glutamic acid, aspartic acid, aspartic acid (DEDD) motif" motif in the active site (Fig. 1*A*). The Mg_A^{2+} ion is essential for recruitment, activation, and positioning of the nucleophilic water molecule that attacks the phosphodiester bond of the substrate, whereas Mg_B^{2+} stimulates product formation. Structural studies with *Bacillus halodurans* RNase H1 demonstrate that the Mg_A^{2+}-binding site is only occupied appreciably in the enzyme–substrate (ES) complex (5).

The overall protein folds and active sites of RNases H1 are well conserved in all branches of life, yet there are significant differences between the RNases H of prokaryotes, eukaryotes, and viruses. While most prokaryotic RNases H contain solely the RNase H domain, the eukaryotic counterpart carries an additional domain, called the RNA–DNA hybrid-binding domain (HBD) (3). The HBD is connected to the RNase H domain by a linker region (Fig. 1*B*). While RNA hydrolysis is catalyzed by the RNase H domain, the HBD enhances RNase H1 substrate-binding affinity and processivity and imparts dimerization upon substrate binding (6).

HIV and hepatitis B virus (HBV) replicate by reverse transcription. They encode homologous type 1 RNase H domains that are necessary for viral replication because they digest the viral genomic RNAs after they are copied into the first DNA strand to permit synthesis of the second DNA strand. Thus, targeting these viral RNases H is a promising therapeutic strategy (7). A potential problem with this strategy is off-target effects. Most inhibitors, including those developed by us targeting HBV (8, 9), could potentially bind to and inhibit human RNase H1, limiting therapeutic use. This is particularly important in the context of viruses that cause chronic infections, such as HIV and HBV, insofar as patients will require long-term treatment.

The α-hydroxytropolone (αHT) compound class is a promising scaffold for development of anti-HIV and anti-HBV RNase H inhibitors, many of which have nanomolar efficacy against the viral RNases H *in vitro* and/or against viral replication (9, 10) with varying degrees of selectivity for the viral enzymes over human RNase H1. Here, we adapted expression of catalytically active human RNase H1 in *Escherichia coli* and determined the mechanism of inhibition of two αHT compounds. In kinetic assays, the inhibitors display kinetic features

* For correspondence: John E. Tavis, john.tavis@health.slu.edu.

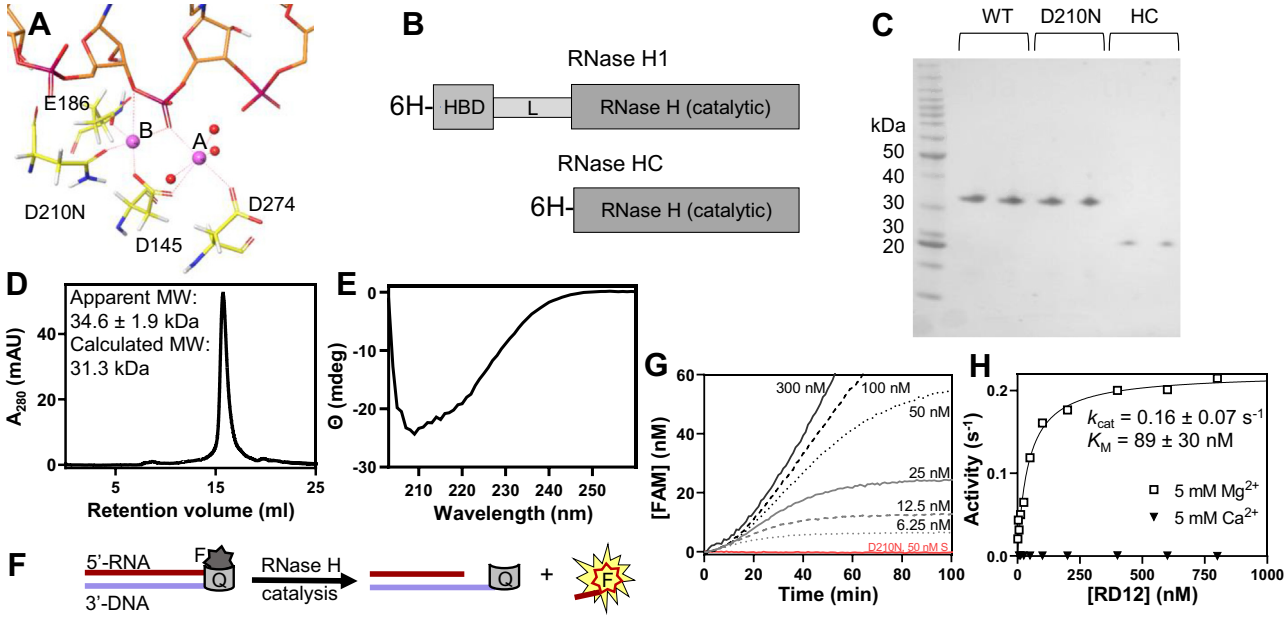

Figure 1. RNase H1 characterization. *A*, RNase H1 active site (PDB: 2QKK) (10) with Mg^{2+} ions *A* and *B* as *blue spheres*, water as *red spheres*, DEDD residues are in *yellow*, and the RNA backbone is in *orange* and *red*. *B*, recombinant gene structures. *C*, SDS-PAGE gel of purified proteins. About 1 μg of protein from two preparations of each protein was electrophoresed in a 4 to 16% gradient gel. Lane 1 is the BenchMark molecular weight marker. *D*, SEC chromatogram of 0.4 ml of 20 μM RNase H1. *E*, CD spectrum of 666 nM RNase H1. *F*, FRET heteroduplex cleavage assay. The *dark star* is quenched fluorescein (*F*), and the *cylinder* is the quencher (Q). Upon cleavage near the 3′ RNA terminus, the fluorescein-labeled fragment is released from proximity to the quencher and fluorescence increases (*yellow star*). *G*, example of RNase H1 (1 nM) reaction progress curves showing concentration of fluorescein (FAM) liberated from quencher over time. Substrate concentrations are indicated. The signal of catalytically inactive mutant RNase $H1^{D210N}$ (50 nM) is at the bottom in *red*. *H*, representative Michaelis–Menten plot for RNase H1 and RD12 fit with the Michaelis–Menten equation $\left(v_0 = V_{max}[S]/K_M+[S]\right)$ (15, 16). Parameters are reported as the mean ± SD of at least three independent measurements. PDB, Protein Data Bank; RNase H1, ribonuclease H1.

reminiscent of noncompetitive inhibition, suggesting that binding of substrate and compounds is not mutually exclusive. Since the compounds bind to the active site, we propose a model in which, by binding to the active site, αHTs stabilize an inactive enzyme–substrate–inhibitor (ESI) complex.

Results

Purification and characterization of human RNase H1

Human RNase H1 (UniProtKB: O60930, amino acids 27–286), a catalytically inactive mutant RNase $H1^{D210N}$, and human RNase HC (amino acids 136–286) containing only the catalytic domain were cloned into a pET-15b vector and expressed in *E. coli* (Fig. 1*B*) (11). All proteins carry an N-terminal histidine tag and thrombin cleavage site. Cells carrying this plasmid exhibited slowed growth, leaky protein expression, and proteolysis of the poorly expressed RNase H1. Addition of 1% glucose to all media resolved these problems without interfering with IPTG-induced expression. Ni^{2+}-affinity purification from cells grown in this manner resulted in protein of >95% purity as determined by SDS-PAGE (Fig. 1*C*) that was free of nucleic acid contamination (absorbance at 260 nm/280 nm = 0.55–0.60). The high purity from one-step purification is due to the proteins' atypically strong binding to the Ni^{2+}–nitrilotriacetic acid resin, which allowed us to add 125 mM imidazole to the wash buffer, greatly reducing nonspecific binding. Size-exclusion chromatography (SEC) revealed a single elution peak corresponding to monomeric RNase H1 with an apparent molecular weight (MW) of 34.6 kDa ± 1.9 kDa (Fig. 1*D*; calculated MW = 31.4 kDa). The yield was ∼2.5 mg per liter of cell culture.

To determine if recombinant RNase H1 is properly folded, we next performed CD experiments in the far-UV range (Fig. 1*E*). The strong negative ellipticity obtained for the human enzyme was similar, yet not identical, to that of the homologous and well-characterized *E. coli* RNase H (12–14). This is consistent with RNase H1 being properly folded and containing ordered secondary structural elements. The difference between *E. coli* and human RNase H1 spectra is likely because the *E. coli* enzyme lacks the unstructured linker and HBD.

Finally, we performed a fluorogenic assay to evaluate the catalytic activity of the recombinant enzyme (Fig. 1*F*). Briefly, we incubated an RNA–DNA hybrid of 12 bp (RD12) labeled with fluorescein at the 3′ RNA terminus and a quencher at the 5′ DNA terminus with the enzyme before adding 5 mM Mg^{2+}. Addition of Mg^{2+} to a solution of 1 nM enzyme and substrate, but not substrate alone, resulted in a significant increase in fluorescence, consistent with separation of the two strands mediated by the enzyme (Fig. 1*G*). Importantly, enzyme activity toward the substrate obeyed Michaelis–Menten kinetics (Fig. 1*H*) (15, 16), implying saturation of enzyme at high substrate concentrations. While the presence of the N-terminal histidine tag did not affect catalytic activity of the enzyme, activity was specific to the presence of Mg^{2+} and residue D210,

since Ca^{2+} did not support catalysis and mutation of D210 to N abrogated its catalytic activity (Fig. 1, *G* and *H*). These data indicate that the recombinant human RNase H1 expressed in *E. coli* and is suitable for biochemical studies.

Inhibition profile of compounds 110 and 404 against human RNase H1

αHTs are RNase H inhibitors that bind to the active site *via* coordination of the divalent metal cofactors. This was determined by cocrystallization of HIV RNase H and the αHT β-thujaplicinol (Fig. 2*A*) (10), which inhibits both HIV and HBV RNase H (17). We focused on two compounds, 110 and 404 (Fig. 2*A*) that are structurally similar to β-thujaplicinol, yet diverse enough to assess the generality of the inhibition mechanism.

To confirm that 110 and 404 bind to metal ions in solution, we performed binding experiments using absorption spectroscopy to monitor complex formation between Mg^{2+} and Ca^{2+} with the compounds (Fig. S1, *A–D*). Mg^{2+} and Ca^{2+} altered the absorption spectra of both compounds substantially, and we determined the compounds' stability constants, *K*, which are related to the dissociation constant (K_D) by the relationship $\log K = -\log K_D$ (Table S1) (18). Two distinct equilibria were observed corresponding to low-affinity and high-affinity binding events, consistent with the compounds' dual metal-chelation motifs (Fig. S1, *E* and *F*). The high-affinity stability constant of Mg^{2+} for 110 ($\log K_1$) was 3.55 (K_D = 0.2 mM), whereas the low-affinity stability constant ($\log K_2$) was 1.61 (K_D = 30 mM). The high-affinity constant is similar to that of the one divalent cation-coordinating dihydroxytropylium ion ($\log K$ = 3.82; K_D = 0.15 mM) (19). Stability constants for 404 were similar to those of 110 ($\log K_1$ = 3.9 and $\log K_2$ = 1.7).

Next, to characterize the inhibitory profiles of the compounds against RNase H1, we titrated the compound and substrate against the enzyme in steady-state kinetics experiments. Kinetic and inhibition parameters are shown in

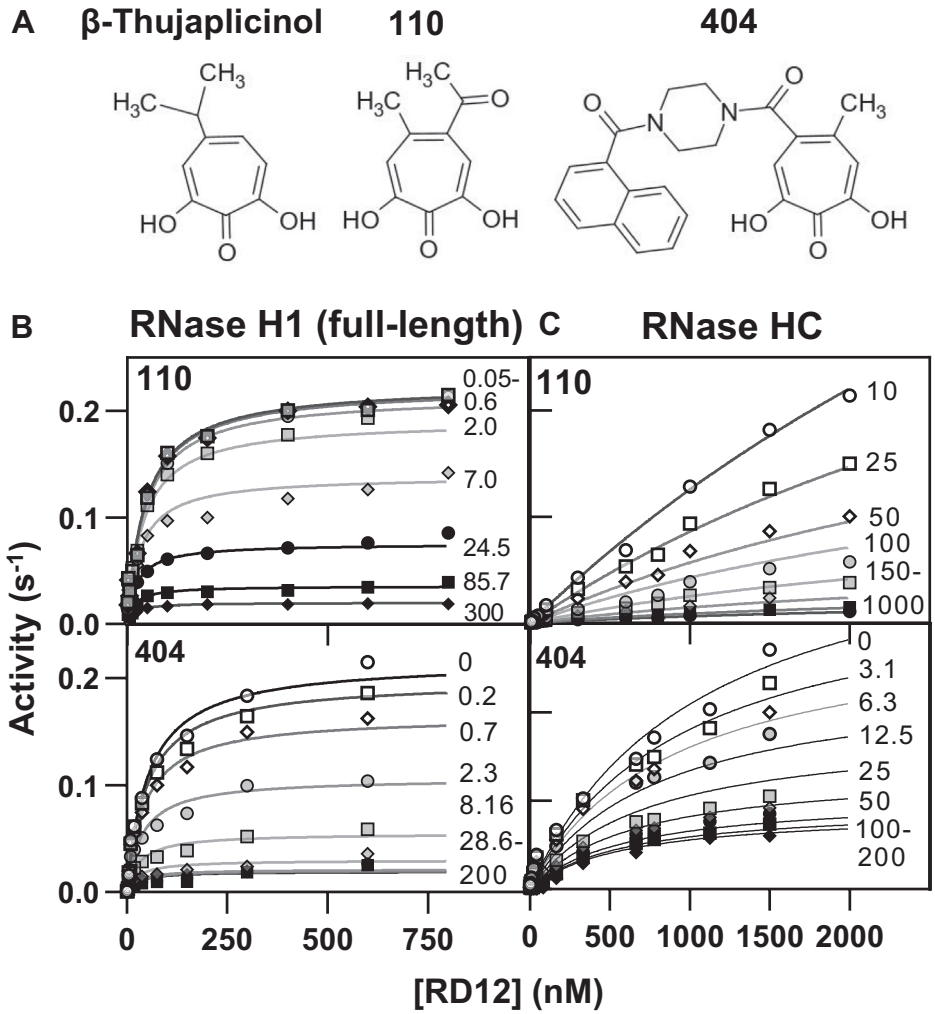

Figure 2. Inhibition kinetics of RNase H1 cleavage of RD12 substrate by compounds 110 and 404. *A*, structures of β-thujaplicinol and compounds 110 and 404. *B* and *C*, representative Michaelis–Menten plots of RNase H1 (*B*) and RNase HC (*C*) in the presence of compound 110 (*top panels*) or compound 404 (*bottom panels*). Data were fit with Equations 1–3 (20). Numbers to the *right* of the regression lines indicate inhibitor concentrations in micromolar. Parameters are shown in Table 1. Plots are representative of three or more independent experiments with additional data in Figs. S2–S5. RD12, RNA–DNA hybrid of 12 bp; RNase H1, ribonuclease H1.

Table 1
RNase H1 kinetic/inhibition parameters

Parameter	RNase H1-wt	RNase HC
k_{cat} (s^{-1})	0.16 ± 0.07	0.22 ± 0.04
K_M (nM)	89 ± 30	>500[a]
k_{cat}/K_M (M^{-1} s^{-1})	1,800,000	440,000
110 K_{iE} (μM)	17.9 ± 11	38 ± 12
110 α	0.61 ± 0.29	Unstable
110 K_{iES} (μM)	8.5 ± 0.0003	Unstable
110 I_{max} (%)	95 ± 2	∼100
404 K_{iE} (μM)	9.3 ± 8	∼15
404 α	0.39 ± 0.17	Unstable
404 K_{iES} (μM)	2.6 ± 0.5	Unstable
404 I_{max} (%)	94 ± 2	∼100

[a] Because of inability to saturate the RNase HC reaction, k_{cat} is highly extrapolated and K_M could not be reliably determined. Data for alternate substrates in Fig. S5. K_{iE} is the K_i of the inhibitor for the free enzyme and K_{iES} is the K_i for the enzyme–substrate complex. α is the proportionality constant for the two inhibition constants. α = K_{iES}/K_{iE} (21).

Table 1. Data were fit with Equations 1–3 (20). Both compounds showed no evidence of competitive inhibition (Figs. 2*B* and S2, *J* and *K* and Table S2). They instead reduced the turnover (V_{max}) while minimally enhancing the apparent affinity for the substrate (K_M) (Figs. 2*B* and S2 and Table S2). Importantly, saturating concentrations of 110 and 404 could not fully inhibit RNase H1 activity (Figs. 2*B* and S3, *A* and *B* and Table S2), both with maximum fractional inhibition (I_{max}) values of ∼95% (Table 1). Inhibition was reversible, as documented by recovery of enzymatic activity after dilution of the compound (Fig. S3, *E* and *F*) (21). These results argue for a reversible and noncompetitive mechanism of inhibition whereby binding of the substrate and compounds are not mutually exclusive.

Determining the impact of the HBD on inhibition

Human RNase H1 contains an HBD (Fig. 1*B*) that imparts high-affinity substrate binding (6, 22). In addition, binding of the substrate to the HBD could allosterically modulate active-site accessibility. To determine the impact of the HBD on inhibition, we assessed the compounds' inhibition profiles against a mutant enzyme that contains only the catalytic domain, referred to as RNase HC (11). Compounds 110 and 404 inhibited RNase HC in a dose-dependent manner (Figs. 2*C*, S3, *C* and *D* and S4). This confirms that the binding site is in the catalytic domain. Because of the much lower affinity of RNase HC for RD12, we could not saturate the reaction to accurately determine K_M and k_{cat}; however, high 110 and 404 concentrations reduced the K_M to within the measurable range, allowing us to fit the data to a global inhibition model (Equations 1–3) (Figs. 2*C* and S4). Like full-length RNase H1, RNase HC was inhibited in a noncompetitive manner. To further validate this observation, we repeated the same assays with 14-mer and 18-mer hybrid substrates for which RNase HC has a lower K_M. We observed clear noncompetitive inhibition with these substrates (Fig. S5). Assays with 404 using 14-mer (Fig. S5, *A*, *F*, and *G*) and 18-mer (Fig. S5, *B*, *C*, *F*, *H*, and *I*) heteroduplex substrates showed reductions of K_M, whereas the effect of compound 110 on K_M was unclear (Fig. S5, *D*, *F*, and *J*). Thus, both compounds inhibited turnover of RNase HC. This indicates that binding of substrate and compound to the catalytic domain is not mutually exclusive.

Two molecules of RNase H1 bind to one molecule of RD12 heteroduplex substrate

Next, we wanted to determine the effect of the compounds on substrate binding. First, we characterized the binding of RNase H1 to RD12 substrate in the absence of inhibitor. To determine the stoichiometry of human RNase H1, we performed SEC of 20 μM RNase H1 preincubated with 5, 10, and 15 μM of RD12 (Fig. 3*A*) in the presence of Ca^{2+} instead of Mg^{2+} to prevent degradation of the substrate (Fig. 1*H*). In all treatments, we observed a major peak with an apparent MW of 68 kDa, which corresponds to a 2:1 enzyme–substrate complex (E_2S; calculated MW = 71 kDa) (Figs. 3*A* and S6). In the 5 μM RD12/20 μM RNase H1 sample, there were two prominent peaks corresponding to the free enzyme and the E_2S complex.

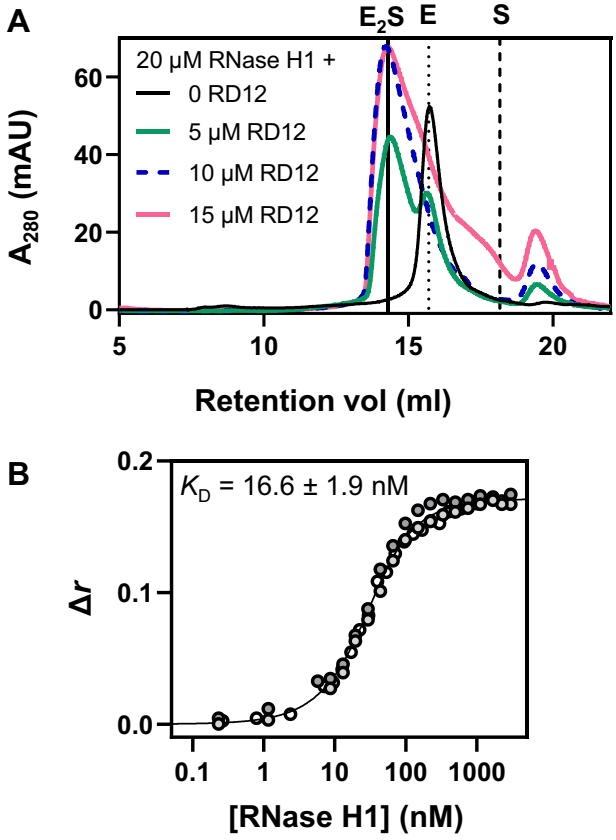

Figure 3. Characterization of the RNase H1–RD12 ES complex. *A*, size-exclusion chromatograms of RD12 substrate titrated against 20 μM RNase H1 in a Superdex 200 increase column with 500 mM NaCl. Superdex 75 chromatograms with 100 mM NaCl and MW standards are shown in Fig. S6*A*. *Vertical lines* indicate retention volumes of the E_2S complex (*solid*; 14.3 ml), the free enzyme (*dotted*; 15.7 ml), and the free substrate (*dashed*; 18.2 ml). Chromatograms are representative of at least two independent experiments. *B*, fluorescence polarization assay of 12.5 nM fluorescein-labeled 12-bp heteroduplex substrate (RD12) titrated with RNase H1. *Gray-filled*, *black-filled*, and *white-filled circles* represent data from three independent experiments. Data were fit with Equation 4 (23). ES, enzyme–substrate; MW, molecular weight; RD12, RNA–DNA hybrid of 12 bp; RNase H1, ribonuclease H1.

Addition of 10 μM RD12 (putatively 20 μM of binding sites) increased the absorption of the E_2S peak and eliminated the free enzyme peak. Finally, addition of 15 μM RD12 did not increase absorption in the E_2S peak, but the 5 μM excess eluted as a shoulder off the side of the ES peak rather than as free substrate, implying that binding is dynamic on the time-scale of the chromatographic run.

To determine substrate-binding affinity, complex formation between RNase H1 and RD12 substrate lacking a quencher on the DNA strand was monitored by fluorescence polarization (FP). Ca^{2+} was again used instead of Mg^{2+}. We titrated RNase H1 against 12.5 nM RD12 and fit the anisotropy data with the quadratic binding equation (Equation 4) (23), which accounts for ligand depletion, in this case RNase H1, when the receptor (RD12) concentration (R_{tot}) is near or above the K_D. R_{tot} was constrained to 25 nM because of the 2:1 stoichiometry (Fig. 3*A*) (6). This yielded a K_D of 16.6 ± 1.9 nM (Figs. 3*B* and S7, *A* and *B*). An approximately fivefold lower K_D relative to the K_M (Fig. 1*H*) is likely because of differences in assay conditions between the kinetics and binding experiments (*e.g.*, Mg^{2+} *versus* Ca^{2+}).

Finally, to independently confirm the stoichiometry of the complex determined by SEC, titrations were performed at 375 nM of RD12 substrate, which is saturating for the enzyme based on K_D = 16.6 nM. After fixing the K_D to 16.6 nM, the calculated concentration of binding sites was 724 nM, which, consistent with a 2:1 stoichiometry, is twice the concentration of the substrate (Fig. S7, *C* and *D*). Together, these results indicate that two molecules of RNase H1 bind one molecule of RD12 with high affinity.

Compounds 110 and 404 modulate substrate binding

Even though most of the inhibitory effects of the αHTs was on V_{max}, compounds 110 and 404 reduced K_M in steady-state kinetics (Figs. 2 and S2, S4 and S5). This is consistent with the observation that β-thujaplicinol binds to the HIV-1 reverse transcriptase (RT):substrate complex with higher affinity than to the free enzyme (10). However, if the assumption that k_{cat} << substrate release (k_{off}) is not true for the RNase H1 mechanism, then the modest reductions in K_M observed here could be due to inhibition of chemical cleavage, product release, or any other zero-order step in the mechanism. To directly assess the compounds' effects on substrate binding, we measured the binding of RNase H1 to substrate with FP as described previously (Fig. 3*B*) in the presence of saturating concentrations of 110 (200 μM), 404 (200 μM), or 2% dimethyl sulfoxide (DMSO) as a control. Compound 110 reduced the K_D approximately threefold, from 12.2 to 4.1 nM (Fig. 4), indicating enhanced affinity. By contrast, the presence of saturating concentrations of compound 404 (200 μM) increased the K_D value sevenfold from 12.2 to 84 nM, indicating loss of affinity (Fig. 4). This result is surprising as it is inconsistent with the K_M reduction observed with the treatment of compound 404 in the kinetics experiments (Figs. 2 and S2, S4 and S5). We suspect this is an artifact from the use of Ca^{2+} instead of Mg^{2+}. Hence, in the presence of Ca^{2+},

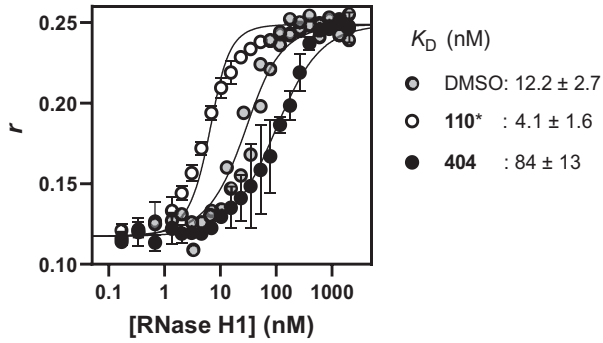

Figure 4. Impact of compounds 110 and 404 on RNase H1–substrate binding. Binding curves for RNase H1 against 12.5 nM RD12 are shown in the presence of 200 μM of compounds 110 and 404 or 2% DMSO. Data were fit with Equation 4 (23). K_D values are the mean and SD of at least four independent measurements. Error bars indicate SD of two independent experiments (more data are shown in Fig. S7). *The measured K_D of compound 110 is the upper limit of K_D. Additional data are shown in Fig. S7, *E* and *F*. DMSO, dimethyl sulfoxide; RD12, RNA–DNA hybrid of 12 bp; RNase H1, ribonuclease H1.

the two structurally similar compounds had opposite effects on substrate binding.

To further explore this unexpected observation, we evaluated the effect of saturating compounds 110 and 404 (500 μM) on the distribution of free RNase H1 and RNase H1 complexed with RD12 using SEC. Ca^{2+} was used to prevent catalysis as in FP assays. We adjusted conditions such that the complex partially dissociated (∼50%) during elution. This involved reducing the enzyme and substrate concentrations to 2.5 and 1.25 μM, respectively. In 100 mM NaCl, the complex did not dissociate during elution, so 500 mM NaCl was added to the sample and elution buffers, which resulted in ∼50% dissociation of enzyme and substrate. Unexpectedly, when scouting conditions to cause partial ES dissociation during SEC, the peak of the complex shifted to an apparent MW of 43 kDa (Figs. 5 and S6, *B–D*) upon reduction of enzyme and substrate concentrations to or below 5 and 2.5 μM, respectively, corresponding closely to the calculated MW of a 1:1 RNase H1–RD12 complex (calculated MW = 39.5 kDa). This could be due to preference of a 1:1 complex at subsaturating concentrations.

To monitor the substrate's elution profile, we measured fluorescein's absorption (absorbance at 485 nm) from the labeled RD12 substrate simultaneously with absorbance at 280 nm, which detects both enzyme and substrate. The enzyme and substrate were preincubated with or without 500 μM of compound 110 or compound 404, and then the complexes were resolved by SEC. We observed a peak in both absorbances at 280 and 485 nm corresponding to the ES complex and two additional peaks and shoulders of 485 and 280 nm, respectively. One of the additional peaks aligns just ahead of the free RD12 retention volume and one just after (Fig. 5*A*). The middle peak of the 485 nm absorbance trace likely comes from free substrate released from the ES complex as it was diluted in the column, and the last peak may arise from single-stranded oligonucleotides, which dissociated as the 12 bp heteroduplex was diluted in the column. Addition of 500 μM of compound 110 to the sample buffer shifted the distribution of free and bound substrate almost entirely to the bound form

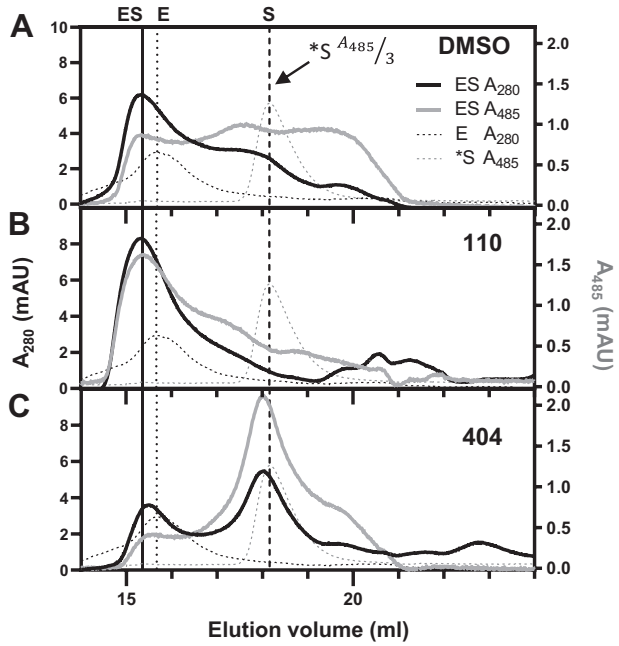

Figure 5. Size-exclusion chromatography (SEC) of ES complex pre-incubated with compound 110 or compound 404. *A*, SEC of 2.5 μM RNase H1 preincubated with 1.25 μM RD12 (ES). The absorbance at 280 nm is represented by *solid black lines*, and the absorbance at 485 nm (fluorescein) by *solid gray lines*. Both absorbances are measured simultaneously. Reference chromatograms of 2.5 μM enzyme (E; *dashed black*; absorbance at 280 nm) and 1.25 μM substrate (S; *dashed gray*; absorbance at 485 nm) assayed independently are shown. *Absorbance at 485 nm signal of this substrate-only control is expressed as absorbance at 485 nm divided by 3 to maintain scale. *B*, SEC of ES as in (*A*) with 500 μM compound 110 or (*C*) 500 μM compound 404. All buffers contain 2% DMSO. *Vertical lines* indicate the retention volumes of the putative 1:1 ES complex (*solid*, 15.3 ml), free RNase H1 (*dotted*; 15.7 ml), and free RD12 substrate (*dashed*; 18.2 ml). Chromatograms are representative of two or more experiments. DMSO, dimethyl sulfoxide; ES, enzyme–substrate; RD12, RNA–DNA hybrid of 12 bp; RNase H1, ribonuclease H1.

(Fig. 5*B*). The same experiment performed with 500 μM of compound 404 resulted in enhanced dissociation of the ES complex, indicated by reduced absorbance at 280 nm at the ES retention volume with the absorbance at 485 nm mostly shifted to the free-substrate position (Fig. 5*C*). Thus, results from SEC are consistent with the enhanced binding observed in the presence of compound 110 and inhibited binding in the presence of compound 404 (Fig. 4). These results support the finding that compound 110 enhances substrate binding in kinetics assays, and competition of compound 404 with substrate in binding assays is likely an artifact of using Ca^{2+} instead of Mg^{2+}.

Modeling of ESI ternary complexes with compounds 110 and 404

To understand how the compounds could produce the inhibition patterns and effects on substrate binding we observed, we employed induced-fit docking of the compounds to RNase H1 (Protein Data Bank [PDB] ID: 2QKK) using the Schrödinger software suite. We constrained our analyses to poses in which the compounds chelate both divalent ions *via* their oxygen trident because the metal-chelating binding mode is well established for the αHTs and RNase H (10). We observed multiple binding poses for compound 110 in the active site (Fig. S8*A*). The hydroxylated tropolone ring of compound 404 bound the Mg^{2+} ions in the active site in a single pose (Fig. S8*B*), but its large appendage docked along the substrate-binding groove outside the active site in different poses. The average predicted binding energy of all poses for compound 110 is −8.2 ± 0.6 kcal/mol and that of compound 404 is −9.2 ± 1 kcal/mol (Fig. S8). Superposition of the 14-mer RNA:DNA heteroduplex substrate from the original RNase H1-substrate cocrystal structure showed that the compounds and the RNA strand cannot simultaneously occupy the active site (Fig. 6), and that compound 404 much more substantially overlapped with the total substrate-binding interface than compound 110. This suggests that the substrate and/or enzyme change their conformation to accommodate the compounds in the active site while remaining bound *via* ES contacts that remain accessible. This seems to be the case with β-thujaplicinol and HIV RNase H (10), where the substrate is predicted to stay just above the active site, interacting with the compound. Compound 404 would require a larger accommodation on the part of the substrate. We suspect the binding poses could be substantially different in the presence of Ca^{2+}, with changes in the binding pose of compound 404 likely having greater effects than changes in the pose of compound 110, by virtue of its larger size.

Discussion

RNase H1 is increasingly being recognized as a central player in nuclear and mitochondrial genome maintenance and replication (1, 24). The consequences of RNase H1 knockout or loss-of-function mutations are severe (2, 25), and therefore, it is important that highly selective antiviral RNase H inhibitors be developed to avoid off-target human RNase H1 inhibition. In addition, αHTs and other metal-chelating compounds can inhibit other DEDD motif–containing viral nucleases, including pUL30/pUL42 of herpes simplex virus 1 and herpes simplex virus 2 (26), HIV integrase (27), the influenza and bunyavirus cap-snatching enzymes (28), and others. Therefore, understanding inhibition of RNase H1 by divalent metal-chelating compounds, including αHTs, will aid development of selective inhibitors of enzymes that share structural or enzymatic similarity with it.

Binding of RNA–DNA hybrid substrate by RNase H1

We showed that human RNase H1 binds to an RD12 with high affinity (K_D = 16.6; Fig. 3*B*) and 2:1 stoichiometry with SEC (Fig. 3*A*) and stoichiometric titration (Fig. S7, *C* and *D*). This is consistent with the 2:1 stoichiometry of the homologous murine RNase H1 (6), though the human enzyme may form 1:1 complexes in subsaturating enzyme and substrate concentrations (Figs. 5*A* and S6, *B–D*). Previous studies (6) show that the catalytic domain on its own binds substrate with lower affinity than the full-length protein, which is consistent with the elevated K_M of RNase HC observed here (Figs. 2*C*, S4

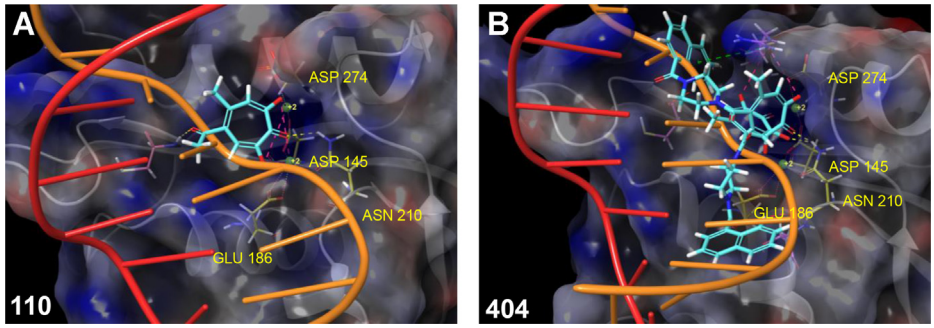

Figure 6. Docking of compound and substrate into the RNase H1 active site. *A* and *B*, induced-fit docking was used to dock compound 110 (*A*) and compound 404 (*B*) into the RNase H1 active with Mg^{2+} inserted where the Ca^{2+} ions were in the original structure (PDB ID: 2QKK). One pose of compound 110 and two poses of compound 404 are shown. The substrate from the original cocrystal structure was then superposed on the enzyme–inhibitor complex. DEDD residues are in *yellow* with D210 replaced with N. PDB, Protein Data Bank; RNase H1, ribonuclease H1.

and S5 and Table 1). RNase H1 contacts its substrate *via* the large binding interfaces of the RNase H domain and HBD (11, 22). Though no structures of the full eukaryotic RNase H1 exist, models have been proposed, most envisioning the enzyme as two balls connected by a string, corresponding to the globular RNase H domain and HBD and the putatively unstructured linker (Fig. 7) (22, 29). The HBD is thought to tightly anchor the enzyme to the substrate while the RNase H domain makes processive cleavages, repeatedly engaging and disengaging the substrate. Furthermore, the single-domain *E. coli* RNase H was recently shown to exhibit processivity (30), from which it follows that the RNase H active site must be empty for some time between processive cleavages while the rest of the enzyme remains bound. Thus, even in the context of the ES complex, there should be opportunities for the compounds to bind.

Compounds 110 and 404 are nontraditional noncompetitive inhibitors

Steady-state kinetics data for compounds 110 and 404 were inconsistent with competitive inhibition, showing strong reductions in V_{max} (Fig. 2). Both compounds also caused modest but significant reductions in K_M. Thus, a rigorous description of the kinetics data requires the general (mixed) model of inhibition (Equations 1–3) (20). In this model, α is the ratio of K_i for the ES complex (K_{iES}) to K_i for the free enzyme (K_{iE}) (21). A minimum V_{max} term was added in the modeling to account for incomplete inhibition in saturating compound and substrate concentrations (Equation 2). This model fits the data of both compounds significantly better than the simple competitive, uncompetitive, and noncompetitive models (Table S2 and Fig. S2, *J* and *K*), most often with $p < 0.01$. Data from RNase HC, which lacks the linker and HBD, also displayed noncompetitive inhibition, with both compounds reducing V_{max} (Figs. 2*C*, S4 and S5) and compound 404 also reducing K_M (Fig. S5, *A*–*C*). Finally, we ruled out irreversible inhibition (Fig. S3, *E* and *F*).

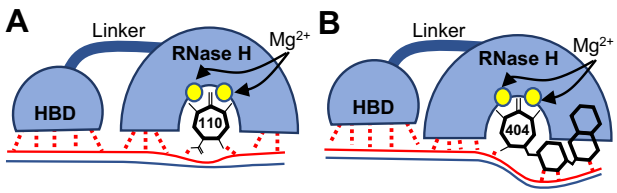

Figure 7. Model for the effects of compounds on substrate binding in the RNase H1 active site. *A* and *B*, models of compound 110 (*A*) and compound 404 (*B*) binding to the Mg^{2+}-bound enzyme–substrate complex. *Solid red line* = RNA, *solid blue line* = DNA, and *dashed red lines* = proposed interactions of substrate with enzyme and inhibitor within the ESI complex. ESI, enzyme–substrate–inhibitor; RNase H1, ribonuclease H1.

In noncompetitive inhibition, the compound may bind to the free enzyme and the ES complex. Noncompetitive kinetics have traditionally been seen as an evidence that the compound binds somewhere other than the active site, causing a conformational change in the enzyme that reduces the turnover rate and may also modulate substrate binding (21). However, active-site binding *via* metal chelation is well established for αHTs with HIV RNase H (10), and an intact two metal-chelating oxygen trident on the inhibitors is essential for their function against all RNases H (31–33). We demonstrated that compounds 110 and 404 bind Mg^{2+} and Ca^{2+} in solution using UV–visible absorption spectroscopy (Fig. S1 and Table S1). Finally, molecular modeling studies support the two-metal ion–bound active sites as the compound-binding site (Fig. S8). From these data, we conclude that compounds 110 and 404 do not work by the mechanism typically inferred from noncompetitive inhibition kinetics.

Instead, experimental data and docking results for both compounds are consistent with compounds binding in the active site as expected but forming stable and inactive ESI complexes rather than competing with the substrate (Fig. 7). Docking studies indicate that substrate and compound cannot bind in the active site at the same time (Fig. 6, (10)). With compound bound, the substrate may bind in an altered conformation, exchanging bonds with RNase H1 active-site residues and Mg^{2+} ions for bonds with the compound. This would account for the noncompetitive kinetics and the enhanced substrate binding. Compound 110 enhanced substrate binding in both kinetics and binding assays, whereas compound 404 was competitive in binding assays while reducing K_M in kinetics assays (Figs. 2, 4 and 5). The reason for this apparent discordant result is uncertain, though Occam's razor suggests it is related to the use of Mg^{2+} in kinetics assays and Ca^{2+} in binding assays. Ca^{2+} has a larger atomic radius

than Mg^{2+} (34), and because of this, the A-site Ca^{2+} ion is displaced from the position of the A-site Mg^{2+} ion, and the two Ca^{2+} ions are substantially further apart than are the two Mg^{2+} ions (35). Ca^{2+} is also more flexible in its number of coordination partners than Mg^{2+}. Finally, the stability constants of Ca^{2+} for compound 110 ($\log K_1$ = 2.56, $\log K_2$ = 0.35) were much lower than those of Mg^{2+} ($\log K_1$ = 3.46, $\log K_2$ = 1.61) (Table S1 and Fig. S1). This indicates differences in how the compounds interact with the two cations that may be relevant to their effects on substrate binding.

It is not clear why saturating concentrations of compound 110 or compound 404 did not cause 100% inhibition of catalysis (Figs. 2, S2 and S3 and Tables 1 and S2). One possibility is that there may be one or more step(s) that occur in assembly of the ESI complexes that have some probability of substrate cleavage. Mg^{2+} stimulates binding of αHTs to the RNase H type 1 active site (10), but the A-site Mg^{2+} ion ($Mg_A{}^{2+}$) does not bind efficiently in the absence of bound substrate (5). Thus, it may be necessary for the substrate to enter the active site to recruit $Mg_A{}^{2+}$ and then partially dissociate to create the two Mg^{2+} ion–bound active site to which the compounds bind most efficiently. After $Mg_A{}^{2+}$ recruitment, the substrate may be cleaved and released from the active site or released uncleaved. We speculate that the compounds may bind immediately after the substrate is released from the active site and form an ESI complex. However, if recruitment of $Mg_A{}^{2+}$ by substrate precedes compound binding to the ES complex, then there would be residual activity related directly to the chance of cleavage when $Mg_A{}^{2+}$ is recruited and inversely to the stability of the ESI complex.

Comparison of human RNase H1 inhibition to viral RNase H inhibition

The αHT β-thujaplicinol (Fig. 2*A*) inhibits HIV-1 RT–associated RNase H in a reversible noncompetitive manner (10), and the compound also exhibited improved binding in the presence of substrate. This is consistent with our finding that inhibition of αHTs 110 and 404 against RNase H1 is greatest in saturating substrate concentrations (*i.e.*, $K_{iES} < K_{iE}$) (Fig. S3, *A–D* and Table 1). The RNases H of both HIV and HBV are domains of larger polymerase proteins with much of their substrate-binding capacity located in their adjacent RT domains (36, 37), recapitulating through a different structural mechanism the overall situation observed with RNase H1. Thus, the mostly noncompetitive behavior of β-thujaplicinol against HIV RT–associated RNase H is because the small β-thujaplicinol molecule does not block a substantial fraction of the total ES contacts. While the mechanism of inhibition of HBV RNase H by αHTs has not been determined because of difficulties in producing suitable recombinant enzyme, the HBV enzyme may also be inhibited in a noncompetitive manner.

Experimental procedures

Protein expression and purification

Full-length RNase H1 (UniProtKB: O60930, amino acids 27–286) and a catalytic domain–only mutant (RNase HC; UniProtKB: O60930, amino acids 136–286) were purified by Ni^{2+}-affinity chromatography as before with modifications (11). Transformed *E. coli* (LOBSTR) were grown and induced in LB media with 1% glucose. 2-Mercaptoethanol was replaced with 1 mM Tris(2-carboxyethyl)phosphine (TCEP) in purification buffers. After Ni^{2+}–nitrilotriacetic acid purification, the buffer was exchanged *via* centrifugal desalting columns into storage buffer (50 mM Hepes, pH 7.5, 400 mM NaCl, 10% glycerol, and 2 mM TCEP) and stored at −80 °C. Proteins were quantified by UV spectroscopy with absorbance at 280 nm molar extinction coefficients of 47,440 M^{-1} cm^{-1} for full-length RNase H1 and 31,970 M^{-1} cm^{-1} for the catalytic domain–only mutant (RNase HC). These values were determined by ExPASy ProtParam using the amino acid sequences of RNase H1 and RNase HC.

CD

Three milliliters of 666 nM RNase H1 in CD buffer (6.25 mM Tris, pH 7.5, 100 mM NaF, 10% glycerol, and 2 mM TCEP) was read in a 10 mm × 10 mm quartz cuvette with an Applied Photophysics CD spectrophotometer at 20 °C. Four sets of 10 reads were taken and averaged. The buffer signal was read and subtracted from the protein sample's signal.

SEC of RNase H1 and ligands

RNase H1, substrate, and compound were run alone and in different combinations. All SEC experiments were conducted in a Superdex 200 Increase 10/300 GL column at room temperature, except in Fig. S6*A*, in which a Superdex 75 10/300 GL was used. The final composition of the elution buffer was 50 mM HEPES, 500 mM NaCl, 10% glycerol, and 2 mM TCEP. The pH was adjusted with NaOH to 7.5. NaCl was reduced to 100 mM in Fig. S6*A*. Buffer stocks were prepared and stored at room temperature without TCEP. A freshly thawed aliquot of HEPES-buffered TCEP (pH 7.5) was added to fresh buffer stock every 2 to 3 h. Each day, ≥40 ml fresh buffer was used to equilibrate the column. Runs were conducted at a flow rate of 0.5 ml/min. Samples were prepared and incubated at room temperature for 15 min prior to starting the run. The sample (0.4 ml) was loaded into the sample loop for each run. Concentrations of enzyme and substrate employed are indicated in the figures. In all experiments using inhibitors, 500 μM of the compound was added to the sample buffer and 2% of DMSO to vehicle controls. Apparent MWs were determined by resolving a set of Bio-Rad gel filtration standards in the same conditions. Average apparent MWs of elution peaks were determined from three or more independent experiments.

Heteroduplex substrate preparation

Fluorescein-labeled RNA oligonucleotides and complementary Iowa Black–labeled DNA oligonucleotides were purchased from Integrated DNA Technologies with HPLC purification. RNAs and DNAs were dissolved in nuclease-free water and combined in a RNA:DNA ratio of 1:1.1 in 50 mM HEPES, pH 7.5, 100 mM NaCl, and 2 mM TCEP. The

substrate solution was heated to 90 °C for 10 min and slowly cooled to 4 °C to promote annealing. For RD12, the RNA sequence is GACACCUGAGUC/36-FAM and the DNA sequence is 5IABkFQ/GACTCAGGTGTC. Additional sequences are shown in Fig. S5*E*.

Compound sourcing

RNase H inhibitors were synthesized by Dr Ryan Murelli (Brooklyn College, City University of New York) (17, 38). Compounds were >95% pure, dissolved at 25 mM in 100% DMSO, and stored in small aliquots at −25 °C in opaque tubes.

RNase H heteroduplex cleavage assay

RNase H reactions were assembled by combining enzyme and substrate in a buffer of 50 mM HEPES, 100 mM NaCl, 2 mM TCEP, and bringing the mixture to 90% final volume with nuclease-free water. Reactions were initiated by adding 2.5 μl of 50 mM $MgCl_2$ to 22.5 μl of the 90% reaction mixture for a final $MgCl_2$ concentration of 5 mM in 25 μl. Assays were assembled at room temperature and conducted at 28 °C in 384-well black plates, and fluorescence was detected at 10 to 60 s intervals in a Biotek Synergy HTX plate reader using 485/20 nm and 528/20 nm filters. Fluorescence of substrate concentration–matched no-catalysis controls lacking either RNase H1 or Mg^{2+} was subtracted from each reaction progress curve at each time point. Maximum rates of fluorescence increase in relative fluorescence units were determined from five or more data points by the Biotek Gen5 3.10 or 3.11 software (BioTek). A linear standard curve was used to convert fluorescence units to nanomolar of released fluorescein by plotting the plateaus of reaction progress curves against RD12 concentration.

Steady-state kinetics inhibition assays

A binary titration was conducted using 12 substrate concentrations spanning the enzyme's K_M and eight inhibitor concentrations spanning the compounds' IC_{50}s, along with a DMSO-matched control and a no-enzyme control for background subtraction. These assays employed RNase H1 at 0.1 to 1 nM or 20 to 40 nM RNase HC. Rates were plotted as a function of substrate concentration for each inhibitor concentration. The compounds do not absorb in the range of fluorescein's excitation or emission; so, no corrections for inner-filter effect were necessary. Data were fit to global models of noncompetitive, uncompetitive, and mixed inhibition in GraphPad Prism (GraphPad Software, Inc). The fits were statistically compared with the extra sum-of-squares *F* test in GraphPad Prism to determine the best-fitting model (Supplementary information and Tables S2–S4). Models were also compared when a minimum V_{max} term ($V_{max_{min}}$) was introduced to account for incomplete inhibition in saturating compound concentrations. We tested whether this term significantly improved the fit by the extra sum-of-squares *F* test. Final data analysis was carried out with the mixed inhibition model (Equations 1–3) (20). All parameters were left free but shared between all datasets within an experiment.

$$v_0 = \frac{V_{max_{app}}[S]}{K_{Mapp} + [S]} \tag{1}$$

$$V_{max_{app}} = V_{max_{min}} + \left[\frac{V_{max_{max}} - V_{max_{min}}}{\left(1 + \frac{[I]}{\alpha * K_i}\right)}\right] \tag{2}$$

$$K_{M_{app}} = K_M * \left[\left(1+\frac{[I]}{K_i}\right) \Big/ \left(1+\frac{[I]}{\alpha * K_i}\right)\right] \tag{3}$$

Where $V_{max_{app}}$ is the V_{max} in the presence of a particular inhibitor concentration, $V_{max_{max}}$ is the V_{max} in the absence of inhibitor, $V_{max_{min}}$ is the V_{max} when inhibition reaches saturation, K_M is the Michaelis constant, $K_{M_{app}}$ is the K_M in a particular inhibitor concentration, K_i is the inhibition constant, α is the proportionality constant between the inhibition constant for the free enzyme relative to the ES complex ($\alpha = K_{iES}/K_{iE}$) (21), v_0 is the initial velocity, and $[I]$ and $[S]$ are inhibitor and substrate concentrations, respectively. Maximum rates of fluorescein release are reported as k_{cat} ($k_{cat} = V_{max}/[E]$). Equations are from Ref. (20) as in GraphPad Prism.

FP substrate-binding assays

RNase H1 was titrated against a fixed concentration of RD12 substrate consisting of fluorescein-labeled RNA and unlabeled DNA in 50 mM HEPES, pH 7.5, 100 mM NaCl, 10% glycerol, 2 mM TCEP, and 5 mM $CaCl_2$. The RD12 concentration was 12.5 nM unless indicated otherwise. After setup, reactions were incubated for 15 min at 28 °C before reading. Polarized fluorescence was read in black 384-well plates with nonbinding surface treatment with a BioTek Synergy H1. Anisotropy was computed in BioTek Gen5 3.11 software. Raw or background-subtracted anisotropy values (r) were fit with Equation 4 (23). R_{tot} was constrained to twice the RD12 concentration because the stoichiometry of RNase H1 for RD12 is 2:1 (Fig. 3*A*, (6)). For K_D determination with inhibitors, 200 μM of compound 110 or compound 404 or 2% DMSO as a vehicle control were added to the binding assay, and data were analyzed as described previously.

$$\Delta r = r_0 + \Delta r_{max}\left(\frac{[R]_{tot} + [L]_{tot} + K_D - \sqrt{\left([R]_{tot} + [L]_{tot} + K_D\right)^2 - \left(4 \cdot [R]_{tot} \cdot [L]_{tot}\right)}}{2 \cdot [R]_{tot}}\right) \tag{4}$$

where Δr is the anisotropy change at a particular enzyme concentration, Δr_{max} is the maximum change at saturation, r_0 is the anisotropy of free RD12, K_D is the dissociation constant, $[R]_{tot}$ is the total receptor binding-site concentration (*i.e.*, [RD12] × 2), and $[L]_{tot}$ is the total ligand concentration (RNase H1) (Equation 6 in Ref. (23)).

Compound-docking studies

The induced-fit docking protocol of Schrödinger suite (Schrödinger 2021-4 LLC) was used to predict binding conformations of compounds 110 and 404 within the active site of RNase H1. Ligands were prepared with LigPrep (Schrödinger LLC) by the following steps: (1) energy minimization with OPSL4 force field and different deprotonation states of the ligands were generated using Epik; (2) metal-binding sites were defined; and (3) compounds were desalted and tautomerized while retaining chirality. We removed the 14 bp DNA–RNA heteroduplex from the crystal structure of RNase HC (PDB ID: 2QKK) and replaced Ca^{2+} ions present in metal coordination site of RNase HC with Mg^{2+} ions by superposition of the HIV RNase H domain (PDB ID: 1RTD). The RNase H1 structure containing Mg^{2+} ions in the metal-binding sites was prepared with protein preparation wizard in Maestro (Schrödinger LLC). Water molecules that were close to the active-site residues were retained while the remaining molecules were removed, the protein was protonated at pH 7.5 ± 2, hydrogen bonds were assigned with PROPKA (Schrödinger LLC) at pH 7.5, and energy minimization was done with OPSL4 force field. β-Thujaplicinol was placed into the active site of RNase H1 by superposition of the DEDD motif of the HIV RNase H–β-thujaplicinol cocrystal structure (PDB ID: 3K2P) onto that of RNase H1. A receptor grid of 10 Å was generated around the centroid of the bound ligand, which was then used for docking of compounds. Protein refinement was carried out at a Van der Waals radius scaling factor of 0.7 for the protein and 0.5 for the ligand. Twenty poses were retained in the initial docking, residues were refined within 5.0 Å of the ligand poses, and redocking was performed with the best structures within 30.0 kcal/mol and the top 20 overall structures. We then superposed the 14-mer RNA–DNA substrate from the original structure (PDB ID: 2QKK) onto the inhibitor-bound enzyme.

Data analysis and statistics

All nonlinear curve fitting, statistical analyses, and graph creation were performed in GraphPad Prism 9.1.1. Outlying values were omitted based on a 1% Q ROUT test (39).

Data availability

All data are either in the main document or in the supporting information.

Supporting information—This article contains supporting information (18, 20, 21, 40).

Acknowledgments—We thank Alex Berkowitz and Ryan P. Murelli for the compounds used in this study. We also thank Sahiti Kuppa and Edwin Antony for assistance with CD spectroscopy.

Author contributions—N. L. P., N. P., and J. E. T. conceptualization; N. L. P. methodology; N. L. P. and R. T. formal analysis; N. L. P. and R. T. investigation; N. L. P. writing–original draft; R. T., N. P., and J. E. T. writing–review and editing; N. L. P. and R. T. visualization; N. P. and J. E. T. supervision; J. E. T. project administration.

Funding and additional information—This work was funded by the US Department of Defense grant (grant no.: W81XWH-18-1-0307 [to J. E. T.]).

Conflict of interest—The authors declare that they have no conflicts of interest with the contents of this article.

Abbreviations—The abbreviations used are: αHT, α-hydroxytropolone; DMSO, dimethyl sulfoxide; ES, enzyme–substrate; ESI, enzyme–substrate–inhibitor; FP, fluorescence polarization; HBD, hybrid-binding domain; HBV, hepatitis B virus; MW, molecular weight; PDB, Protein Data Bank; RD12, RNA–DNA hybrid of 12 bp; RNase H, ribonuclease H; RNase H1, ribonuclease H1; RT, reverse transcriptase; SEC, size-exclusion chromatography; TCEP, Tris(2-carboxyethyl)phosphine.

References

1. Holt, I. J. (2019) The Jekyll and Hyde character of RNase H1 and its multiple roles in mitochondrial DNA metabolism. *DNA Repair* **84**, 102630
2. Cerritelli, S. M., Frolova, E. G., Feng, C., Grinberg, A., Love, P. E., and Crouch, R. J. (2003) Failure to produce mitochondrial DNA results in embryonic lethality in Rnaseh1 null mice. *Mol. Cell* **11**, 807–815
3. Hyjek, M., Figiel, M., and Nowotny, M. (2019) RNases H: Structure and mechanism. *DNA Repair (Amst)* **84**, 102672
4. Samara, N. L., and Yang, W. (2018) Cation trafficking propels RNA hydrolysis. *Nat. Struct. Mol. Biol.* **25**, 715–721
5. Nowotny, M., Gaidamakov, S. A., Crouch, R. J., and Yang, W. (2005) Crystal structures of RNase H bound to an RNA/DNA hybrid: Substrate specificity and metal-dependent catalysis. *Cell* **121**, 1005–1016
6. Gaidamakov, S. A., Gorshkova, , II, Schuck, P., Steinbach, P. J., Yamada, H., Crouch, R. J., and Cerritelli, S. M. (2005) Eukaryotic RNases H1 act processively by interactions through the duplex RNA-binding domain. *Nucleic Acids Res.* **33**, 2166–2175
7. Edwards, T. C., Ponzar, N. L., and Tavis, J. E. (2019) Shedding light on RNaseH: A promising target for hepatitis B virus (HBV). *Expert Opin. Ther. Targets* **23**, 559–563
8. Edwards, T. C., Mani, N., Dorsey, B., Kakarla, R., Rijnbrand, R., Sofia, M. J., and Tavis, J. E. (2019) Inhibition of HBV replication by N-hydroxyisoquinolinedione and N-hydroxypyridinedione ribonuclease H inhibitors. *Antiviral Res.* **164**, 70–80
9. Li, Q., Lomonosova, E., Donlin, M. J., Cao, F., O'Dea, A., Milleson, B., Berkowitz, A. J., Baucom, J.-C., Stasiak, J. P., Schiavone, D. V., Abdelmessih, R. G., Lyubimova, A., Fraboni, A. J., Bejcek, L. P., Villa, J. A., *et al.* (2020) Amide-containing α-hydroxytropolones as inhibitors of hepatitis B virus replication. *Antivir. Res.* **177**, 104777
10. Himmel, D. M., Maegley, K. A., Pauly, T. A., Bauman, J. D., Das, K., Dharia, C., Clark, A. D., Jr., Ryan, K., Hickey, M. J., Love, R. A., Hughes, S. H., Bergqvist, S., and Arnold, E. (2009) Structure of HIV-1 reverse transcriptase with the inhibitor beta-Thujaplicinol bound at the RNase H active site. *Structure* **17**, 1625–1635
11. Nowotny, M., Gaidamakov, S. A., Ghirlando, R., Cerritelli, S. M., Crouch, R. J., and Yang, W. (2007) Structure of human RNase H1 complexed with

an RNA/DNA hybrid: Insight into HIV reverse transcription. *Mol. Cell* **28**, 264–276
12. Spudich, G. M., Miller, E. J., and Marqusee, S. (2004) Destabilization of the Escherichia coli RNase H kinetic intermediate: Switching between a two-state and three-state folding mechanism. *J. Mol. Biol.* **335**, 609–618
13. Yamasaki, K., Ogasahara, K., Yutani, K., Oobatake, M., and Kanaya, S. (1995) Folding pathway of Escherichia coli ribonuclease HI: A circular dichroism, fluorescence, and NMR study. *Biochemistry* **34**, 16552–16562
14. Dabora, J. M., and Marqusee, S. (1994) Equilibrium unfolding of Escherichia coli ribonuclease H: Characterization of a partially folded state. *Protein Sci.* **3**, 1401–1408
15. Leonor Michaelis, M. M. (1913) Die kinetik der Invertinwirkung. *Biochemische Z.* **49**, 333–369
16. Johnson, K. A., and Goody, R. S. (2011) The original Michaelis constant: Translation of the 1913 michaelis–menten paper. *Biochemistry* **50**, 8264–8269
17. Hu, Y., Cheng, X., Cao, F., Huang, A., and Tavis, J. E. (2013) β-Thujaplicinol inhibits hepatitis B virus replication by blocking the viral ribonuclease H activity. *Antivir. Res.* **99**, 221–229
18. Kocyła, A., Pomorski, A., and Krężel, A. (2017) Molar absorption coefficients and stability constants of Zincon metal complexes for determination of metal ions and bioinorganic applications. *J. Inorg. Biochem.* **176**, 53–65
19. Hirai, M., and Oka, Y. (1970) Stability of tropolone chelates of the Bi- and tervalent metal ions. *Bull. Chem. Soc. Jpn.* **43**, 778–782
20. Copeland, R. A. (2013) Reversible modes of inhibitor interactions with enzymes *Evaluation of Enzyme Inhibitors in Drug Discovery. A Guide for Medicinal Chemists and Pharmacologists*, 2 Ed., Wiley, Hoboken, NJ
21. Strelow J, D. W., Dewe, W., Iverson, P. W., Brooks, H. B., Radding, J. A., McGee, J., and Weidner, J. (2012) Mechanism of action assays for enzymes. In: Markossian., S., Grossman, A., Brimacombe, K., Arkin, M., Auld, D., Austin, C. P., Baell, J., Chung, T. D. Y., Coussens, N. P., Dahlin, J. L., Devanarayan, V., Foley, T. L., Glicksman, M., Hall, M. D., Haas, J. V., *et al*. eds. *Assay Guidance Manual [Internet]*, Eli Lilly & Company and the National Center for Advancing Translational Sciences, Bethesda, MD
22. Nowotny, M., Cerritelli, S. M., Ghirlando, R., Gaidamakov, S. A., Crouch, R. J., and Yang, W. (2008) Specific recognition of RNA/DNA hybrid and enhancement of human RNase H1 activity by HBD. *Embo J.* **27**, 1172–1181
23. Pollard, T. D. (2010) A guide to simple and informative binding assays. *Mol. Biol. Cell* **21**, 4061–4067
24. Parajuli, S., Teasley, D. C., Murali, B., Jackson, J., Vindigni, A., and Stewart, S. A. (2017) Human ribonuclease H1 resolves R-loops and thereby enables progression of the DNA replication fork. *J. Biol. Chem.* **292**, 15216–15224
25. Lima, W. F., Murray, H. M., Damle, S. S., Hart, C. E., Hung, G., De Hoyos, C. L., Liang, X.-H., and Crooke, S. T. (2016) Viable RNaseH1 knockout mice show RNaseH1 is essential for R loop processing, mitochondrial and liver function. *Nucleic Acids Res.* **44**, 5299–5312
26. Tavis, J. E., Wang, H., Tollefson, A. E., Ying, B., Korom, M., Cheng, X., Cao, F., Davis, K. L., Wold, W. S. M., and Morrison, L. A. (2014) Inhibitors of nucleotidyltransferase superfamily enzymes suppress herpes simplex virus replication. *Antimicrob. Agents Chemother.* **58**, 7451–7461
27. Didierjean, J., Isel, C., Querré, F., Mouscadet, J.-F., Aubertin, A.-M., Valnot, J.-Y., Piettre, S. R., and Marquet, R. (2005) Inhibition of human immunodeficiency virus type 1 reverse transcriptase, RNase H, and integrase activities by hydroxytropolones. *Antimicrob. Agents Chemother.* **49**, 4884–4894
28. Kumar, G., Cuypers, M., Webby, R. R., Webb, T. R., and White, S. W. (2021) Structural insights into the substrate specificity of the endonuclease activity of the influenza virus cap-snatching mechanism. *Nucleic Acids Res.* **49**, 1609–1618
29. Lima, W. F., Wu, H., Nichols, J. G., Prakash, T. P., Ravikumar, V., and Crooke, S. T. (2003) Human RNase H1 uses one tryptophan and two lysines to position the enzyme at the 3′-DNA/5′-RNA terminus of the heteroduplex substrate. *J. Biol. Chem.* **278**, 49860–49867
30. Lee, H., Cho, H., Kim, J., Lee, S., Yoo, J., Park, D., and Lee, G. (2021) RNase H is an exo- and endoribonuclease with asymmetric directionality, depending on the binding mode to the structural variants of RNA:DNA hybrids. *Nucleic Acids Res* **50**, 1801–1814
31. Edwards, T. C., Lomonosova, E., Patel, J. A., Li, Q., Villa, J. A., Gupta, A. K., Morrison, L. A., Bailly, F., Cotelle, P., Giannakopoulou, E., Zoidis, G., and Tavis, J. E. (2017) Inhibition of hepatitis B virus replication by N-hydroxyisoquinolinediones and related polyoxygenated heterocycles. *Antivir. Res.* **143**, 205–217
32. Cao, L., Song, W., De Clercq, E., Zhan, P., and Liu, X. (2014) Recent progress in the research of small molecule HIV-1 RNase H inhibitors. *Curr. Med. Chem.* **21**, 1956–1967
33. Tramontano, E., Corona, A., and Menéndez-Arias, L. (2019) Ribonuclease H, an unexploited target for antiviral intervention against HIV and hepatitis B virus. *Antivir. Res.* **171**, 104613
34. Pauling, L. (1947) Atomic Radii and interatomic distances in metals. *J. Am. Chem. Soc.* **69**, 542–553
35. Nowotny, M., and Yang, W. (2006) Stepwise analyses of metal ions in RNase H catalysis from substrate destabilization to product release. *EMBO J.* **25**, 1924–1933
36. Zhang, Z., and Tavis, J. E. (2006) The duck hepatitis B virus reverse transcriptase functions as a full-length monomer. *J. Biol. Chem.* **281**, 35794–35801
37. Tian, L., Kim, M.-S., Li, H., Wang, J., and Yang, W. (2018) Structure of HIV-1 reverse transcriptase cleaving RNA in an RNA/DNA hybrid. *Proc. Natl. Acad. Sci. U. S. A.* **115**, 507
38. Lu, G., Lomonosova, E., Cheng, X., Moran, E. A., Meyers, M. J., Le Grice, S. F., Thomas, C. J., Jiang, J. K., Meck, C., Hirsch, D. R., D'Erasmo, M. P., Suyabatmaz, D. M., Murelli, R. P., and Tavis, J. E. (2015) Hydroxylated tropolones inhibit hepatitis B virus replication by blocking viral ribonuclease H activity. *Antimicrob. Agents Chemother.* **59**, 1070–1079
39. Motulsky, H. J., and Brown, R. E. (2006) Detecting outliers when fitting data with nonlinear regression – a new method based on robust nonlinear regression and the false discovery rate. *BMC Bioinformatics* **7**, 123
40. Jarmoskaite, I., AlSadhan, I., Vaidyanathan, P. P., and Herschlag, D. (2020) How to measure and evaluate binding affinities. *Elife* **9**, e57264